THE JOURNAL OF PHYSICAL CHEMISTRY Letters

pubs.acs.org/JPCL Letter

Eu^{3+} Sensitization via Nonradiative Interparticle Energy Transfer Using Inorganic Nanoparticles

Marie Anne van de Haar,* Anne C. Berends, Michael R. Krames, Liudmyla Chepyga, Freddy T. Rabouw, and Andries Meijerink

Cite This: *J. Phys. Chem. Lett.* 2020, 11, 689–695 Read Online

ACCESS | Metrics & More | Article Recommendations | Supporting Information

ABSTRACT: Phosphors have been used successfully for both research and commercial applications for decades. Eu^{3+}-doped materials are especially promising, because of their extremely stable, efficient, and narrow red emission lines. Although these emission properties are ideal for lighting applications, weak absorption in the blue spectral range has until now prevented the use of Eu^{3+}-based phosphors in applications based on blue light-emitting diodes. Here, we demonstrate a sensitization mechanism of Eu^{3+} based on interparticle Förster resonance energy transfer (IFRET) between lanthanide-doped inorganic nanocrystals (NCs). Compared to co-doping different lanthanides in the same host crystal, IFRET allows an independent choice of host lattices for Eu^{3+} and its sensitizer while potentially greatly reducing metal-to-metal charge transfer quenching. We demonstrate IFRET between NCs, resulting in red Eu^{3+} emission upon blue excitation at 485 nm using $LaPO_4$:Tb/$LaPO_4$:Eu and $LaPO_4$:Tb/$YVPO_4$:Eu NC mixtures. These findings pave the way toward engineering blue-sensitized line emitters for solid-state lighting applications.

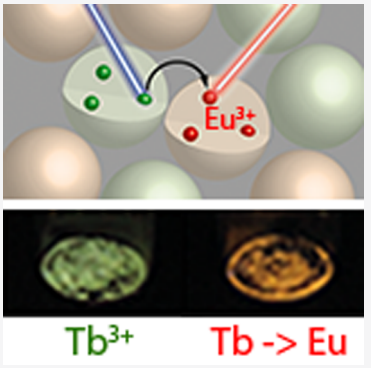

Trivalent lanthanide-doped luminescent materials are of great interest for many applications because of their extremely stable and often narrow emission lines. They not only have been used successfully in fluorescent lighting applications, lasers, optical fibers, imaging, and displays for decades but also are candidates for sensing, labeling, and security applications.[1−5] Despite these successes, narrow-line-emitting trivalent lanthanides have limited suitability if excitation in the visible spectral range is desired, because their absorption is too weak outside the ultraviolet spectral range. For solid-state lighting applications, for example, narrow-line emitters such as Eu^{3+} would have ideal emission properties to boost color rendering and lumen efficacy.[6,7] However, converter materials in solid-state lighting are usually pumped with a violet or blue light-emitting diode (LED), which has so far prevented these ions from being successfully applied in phosphors for white light LEDs.

A promising approach to increase the excitation probability of a lanthanide ion is by using a sensitizer, an optically active ion that strongly absorbs the wavelength of choice and then transfers the absorbed energy to the emitter ion (also called the activator) via nonradiative resonant energy transfer. For example, sensitizer ions like Eu^{2+}, Ce^{3+}, Pb^{2+}, and Bi^{3+} have been considered to effectively enhance the absorption in the blue and sensitize Eu^{3+} emission.[8−14] However, both the absorption properties of the sensitizer and the emission properties of Eu^{3+} depend on the host material. This severely limits the chances of finding a host material in which the sensitizer and Eu^{3+} can be co-doped and both have the desired properties. Another complication of co-doping is quenching of the luminescence, which often occurs in nearest-neighbor pairs of sensitizers and emitters via a metal-to-metal charge transfer state (e.g., Ce^{3+}−Eu^{3+} → Ce^{4+}−Eu^{2+}). This further narrows the selection of the emitter−sensitizer pair and their doping concentrations.

Charge transfer quenching can be circumvented by using energy transfer via energy migration over a concentrated sublattice of a third luminescent ion. This approach has been investigated in the past for Gd^{3+} and Tb^{3+} sublattices.[11,12,15] For example, the principle was reported for Ce^{3+} → $(Tb^{3+})_n$ → Eu^{3+} and Eu^{2+} → $(Tb^{3+})_n$ → Eu^{3+}.[11] In the latter system, increasing the Tb^{3+} concentration leads to more efficient energy migration, and above the percolation point of ∼40% Tb^{3+}, almost all of the migrating energy is captured by Eu^{3+} after excitation of Eu^{2+} at a wavelength (λ) of 377 nm. Although this approach works for high migration ion concentrations, metal-to-metal charge transfer quenching is easily thermally activated and still dominates at elevated temperatures.[11] In addition, energy migration effectively prevents charge transfer quenching only when no back-transfer to the sensitizer ion can occur, which is shown to be problematic for blue-excitable sensitizers such as cerium-doped garnets in combination with, for example, Tb^{3+} or Pr^{3+}.[12,16]

Received: December 18, 2019
Accepted: January 10, 2020
Published: January 10, 2020

https://dx.doi.org/10.1021/acs.jpclett.9b03764
J. Phys. Chem. Lett. 2020, 11, 689–695

Efficient nonradiative energy transfer and suppression of metal-to-metal charge transfer have also been demonstrated by physically separating sensitizer and emitter lanthanide ions in core/shell nanocrystal (NC) geometries[17−26] and have even been suggested for micrometer-sized particles.[27] Core/shell geometries, however, greatly limit the choice of host lattice combinations because the crystal lattice parameters of the materials must be matched.

Here, we introduce a new approach for sensitizing Eu^{3+} emission that circumvents the issues of co-doping Eu^{3+} and a sensitizer into a single host lattice. It relies on interparticle Förster resonance energy transfer (IFRET) that couples nanocrystals (NCs) doped with sensitizer ions and NCs doped with Eu^{3+} (Figure 1). For efficient Förster energy

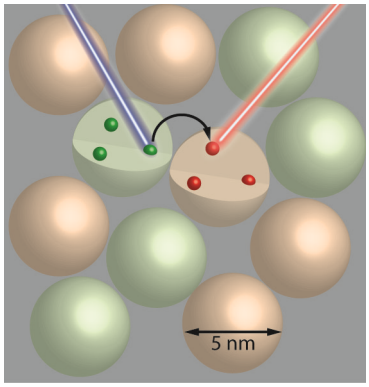

Figure 1. Sketch of the interparticle energy transfer mechanism. Red light is emitted from the Eu^{3+}-doped emitter particle, following excitation of a neighboring nanoparticle doped with Tb^{3+} sensitizer ions. Due to the physical separation of both emitter and sensitizer ions, charge transfer quenching is prevented.

transfer between lanthanide ions, sensitizer−emitter distances on the order of 0.5−1.5 nm are required.[28,29] The concept of IFRET in NC composites provides various tuning knobs to control the distances and transfer efficiencies between sensitizer and emitter ions (see Figure S1). To achieve successful IFRET, we therefore ensure that the NCs in our multihost−lattice composite material are small and in the proximity of each other. Our approach allows an independent choice of the sensitizer and emitter host lattice and prevents charge transfer quenching, which is an even shorter-distance process (<0.5 nm range) than energy transfer via dipolar interactions (0.5−1.5 nm).[11,30,31] IFRET has previously been demonstrated between lanthanide ions only in the same host materials and never with materials that were blue-excitable.[32,33] In this work, we demonstrate efficient sensitization of Eu^{3+} via IFRET from Tb^{3+} ions in different material systems. We show IFRET sensitization in the blue at a λ of 485 nm and achieve IFRET even if the host materials for emitter and sensitizer ions are different. We also demonstrate the robustness of the IFRET-sensitized Eu^{3+} emission intensity from room temperature to 145 °C.

We first tested the homogeneous mixing of the Eu^{3+}-doped emitting NCs and the Tb^{3+}-doped sensitizer NCs. To this end, "wet-mixed" NC composites were compared with "dry-mixed" composites (see Experimental Methods for details). Scanning transmission electron microscopy (STEM) combined with energy dispersive X-ray spectroscopy (EDX) elemental mapping (Figure S2) shows that the NCs are approximately 5−10 nm in diameter with doping concentrations of 10% Eu^{3+} in $YVPO_4$, 40% Tb^{3+} in $LaPO_4$, and 7% Eu^{3+} in $LaPO_4$. High-resolution EDX mappings on $LaPO_4$:Tb/$YVPO_4$:Eu NC composites confirm that the wet-mixed sample is a homogeneous composite of the two types of NCs (Figure 2B,D), showing strong intermixing of the two materials on a

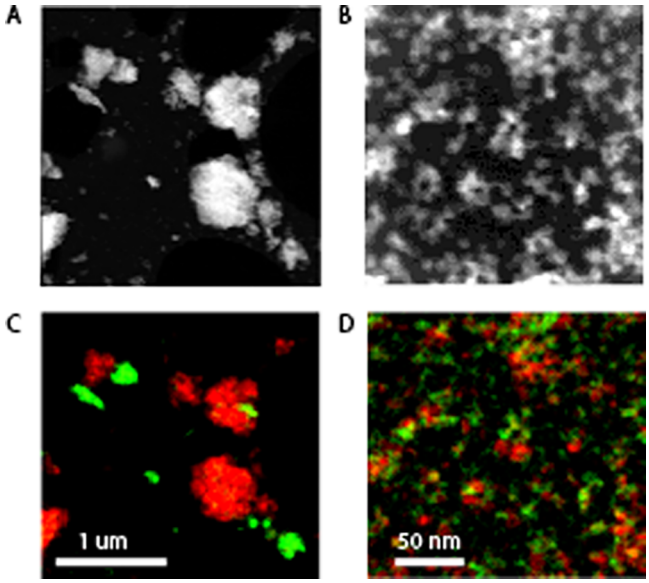

Figure 2. (A and B) HAADF-STEM images and (C and D) STEM-EDX mappings of (A and C) dry-mixed and (B and D) wet-mixed $LaPO_4$:Tb/$YVPO_4$:Eu NCs. Green represents lanthanum (in $LaPO_4$:Tb), and red represents vanadium (in $YVPO_4$:Eu). Clearly, dry mixing results in inhomogeneities at micrometer length scales, while wet mixing produces homogeneous composites.

<10 nm scale. The dry-mixed sample, on the other hand, is largely inhomogeneous (Figure 2A,C), with very little intermixing between the two types of NCs on a scale of less than hundreds of nanometers. More STEM-EDX mappings of these samples are shown in Figure S3. Because FRET between lanthanide ions typically works effectively only for donor−acceptor distances of <1.5 nm, NC intermixing on a scale of a few hundred nanometers is not expected to result in any measurable IFRET signals. We therefore use the dry-mixed sample as a reference without IFRET. The same structural analysis could not be performed on the $LaPO_4$:Tb/$LaPO_4$:Eu mixtures, because it proved to be too difficult to distinguish between these materials using EDX. Nevertheless, our optical measurements (see below) confirm similar structural differences of mixing between wet-mixed and dry-mixed samples for the $LaPO_4$:Tb/$LaPO_4$:Eu composites.

Next, the samples were characterized optically to obtain evidence for interparticle energy transfer. In the case of IFRET, excitation in the $^5D_4$ level of Tb^{3+} will result in red emission from the $^5D_0$ level of Eu^{3+} and give rise to extra Eu^{3+} emission lines, which serves as a fingerprint for IFRET. In excitation spectra of a characteristic Eu^{3+} emission line, the Tb^{3+} $^7F_6$-$^5D_4$ excitation line will appear as a result of IFRET. Figure 3 shows the emission spectra of the wet-mixed and dry-mixed $LaPO_4$:Tb/$LaPO_4$:Eu NC composites upon $^5D_4$ excitation of Tb^{3+} at a λ of 484.5 nm. As a comparison, we also show the emission of the single-component NC composites, $LaPO_4$:Tb and $LaPO_4$:Eu. The single-component $LaPO_4$:Tb NCs show strong emission lines centered at λ values of 540, 590, and 620

https://dx.doi.org/10.1021/acs.jpclett.9b03764
J. Phys. Chem. Lett. 2020, 11, 689−695

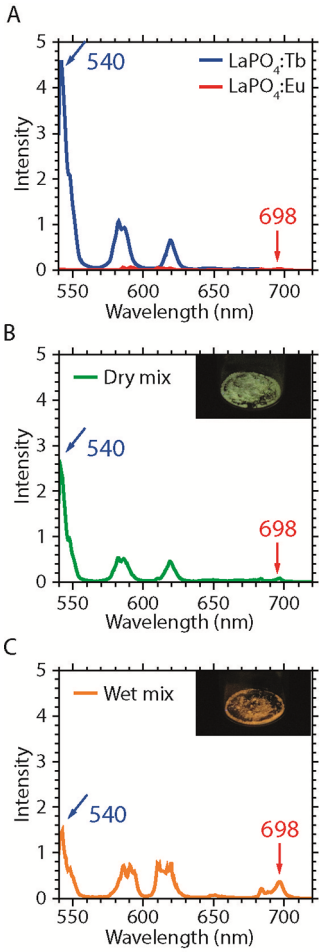

Figure 3. Emission spectra upon Tb^{3+} excitation at a λ of 484.5 nm of (A) single-component $LaPO_4$:Tb (blue) and $LaPO_4$:Eu (red) NC composites and (B) dry-mixed and (C) wet-mixed $LaPO_4$:Tb/$LaPO_4$:Eu NC composites. A Eu^{3+} emission band is observed at a λ of 698 nm in the case of the wet-mixed NCs, indicating Eu^{3+} emission upon Tb^{3+} excitation. The insets in panels B and C show photographs of the luminescence of the dry- and wet-mixed materials upon excitation at 365 nm.

nm, corresponding to the $^5D_4 \rightarrow {}^7F_5$, $^5D_4 \rightarrow {}^7F_4$, and $^5D_4 \rightarrow {}^7F_3$ transitions of Tb^{3+}, respectively. The single-component $LaPO_4$:Eu NCs have almost no luminescence over the entire range when excited at a λ of 484.5 nm as there is no resonant absorption line of Eu^{3+} at this wavelength.

The dry-mixed NC composite shows a reduced Tb^{3+} $^5D_4 \rightarrow {}^7F_5$ emission intensity around 540 nm (Figure 3B) compared to the single-component $LaPO_4$:Tb NCs (Figure 3A). This results from dilution as a result of the 1:1 weight ratio mixing with $LaPO_4$:Eu NCs. For the wet-mixed sample (Figure 3C), the 540 nm emission line is even weaker than for the dry-mixed sample (Figure 3B). In addition, we observe the appearance of new emission lines around 590, 610, and 698 nm that can be ascribed to $^5D_0 \rightarrow {}^7F_1$, $^5D_0 \rightarrow {}^7F_2$, and $^5D_0 \rightarrow {}^7F_4$ emission of Eu^{3+}, respectively. The 590 and 610 nm emissions overlap strongly with Tb^{3+} emission lines, but the 698 nm Eu^{3+} emission is well-separated from Tb^{3+} emission and can serve as a characteristic Eu^{3+} emission line. These observations suggest energy transfer from Tb^{3+} to Eu^{3+} in the wet-mixed NC composite, while the dry-mixed sample does not show indications of IFRET. The differences in IFRET efficiencies for wet- and dry-mixed samples are consistent with our expectations based on structural analysis (Figure 2). This highlights the importance of homogeneous intermixing at the nanometer scale for efficient IFRET. The photographs in the insets of Figure 3 show that the luminescence color difference between the two samples is clearly visible by eye, where the wet-mixed NCs clearly emit more red (Eu^{3+}) light, compared to the dry-mixed NCs that mostly show green (Tb^{3+}) emission.

To confirm preservation of the NC quality during the mixing procedures, the Eu^{3+} emission was measured for direct excitation ($^7F_0 \rightarrow {}^5L_6$) at 395 nm (Figure S4). The Eu^{3+} emission spectrum and intensity are very similar for the wet- and dry-mixed samples, indicating similar mixing ratios and preservation of the $LaPO_4$:Eu NC integrity in the two mixed samples.

Additional evidence for IFRET is found by measuring the excitation spectra of the Eu^{3+} $^5D_0 \rightarrow {}^7F_4$ emission peak at a λ_{em} of 698 nm for both mixtures and for the individual single-component materials (for the pure $LaPO_4$:Tb sample, we monitored at a λ_{em} of 542 nm), as shown in Figure 4. The excitation spectra of dry-mixed NCs and single-component $LaPO_4$:Eu are identical (Figure 4B), confirming the absence of Eu^{3+} sensitization by Tb^{3+}. In contrast, the excitation spectrum of the wet-mixed NCs shows clear evidence of Tb^{3+} excitation lines (most notably, between 340 and 380 nm and at 485 nm), in addition to those originating from Eu^{3+} (most notably, at 395 and 465 nm). This is consistent with IFRET in the wet-mixed sample.

IFRET is a nonradiative decay pathway for the Tb^{3+} $^5D_4$ excited state and will result in faster and non-exponential decay of the $^5D_4$ emission. Measuring luminescence decay curves provides additional evidence for IFRET and helps to quantify the average transfer rate and efficiency. Figure 5 shows decay curves of Tb^{3+} $^5D_4$ emission (λ_{em} = 542 nm). The average lifetimes for the dry- and wet-mixed samples are 1.5 and 0.7 ms, respectively (1/e decay time). The decrease in decay time of the donor emission is a well-known signature for FRET.[34] On the basis of these numbers, we can estimate that the average IFRET rate in our wet-mixed sample is ~0.76 ms^{-1}. Assuming equal nonradiative decay rates from other mechanisms, we can estimate the IFRET efficiency in the wet-mixed sample from the ratio between the integrated areas under the decay curves[35] to be 54%.

To investigate the temperature stability of the IFRET-sensitized emission, emission spectra were recorded upon Tb^{3+} excitation at 485 nm from room temperature to 145 °C (Figure 6). Interestingly, the Eu^{3+} emission stays almost constant within this temperature range. The Tb^{3+} emission shows some thermal quenching behavior. The intensity recovers when the sample is cooled again (Figure S5b). Temperature-dependent excitation spectra (Figure S5c,d) do show some thermal quenching of the Eu^{3+} emission upon direct excitation (e.g., at λ = 395 nm), but not for sensitization via IFRET, which can be explained by a slightly higher IFRET efficiency at elevated temperatures. An incidental increased Eu^{3+} emission intensity is observed at 105 °C but seems to be due to an experimental error, because it is not observed in the "back trace" (see Figure S5b). In addition, the excitation spectra measured at 105 °C (Figure S5c) show enhanced Eu^{3+} emission for not only excitation via energy transfer (i.e., at λ = 485 nm) but also direct excitation (i.e., λ = 395 nm), indicating that the increased Eu^{3+} emission at 105 °C is not the result of enhanced energy transfer efficiencies. For the sake of

https://dx.doi.org/10.1021/acs.jpclett.9b03764
J. Phys. Chem. Lett. 2020, 11, 689−695

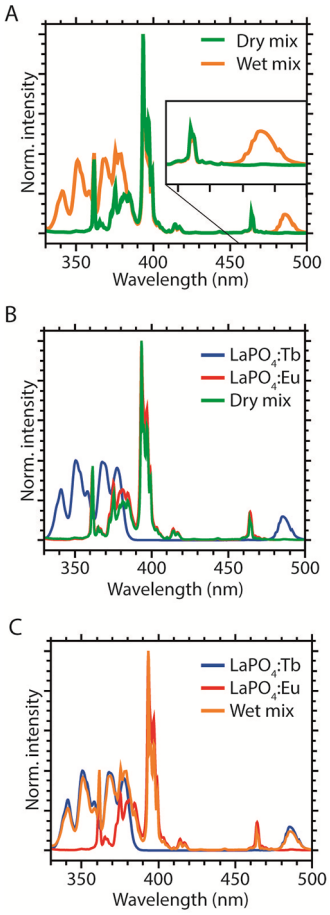

Figure 4. Excitation spectra of Eu^{3+} emission, monitored at a λ of 698 nm, of (A) dry-mixed (green) and wet-mixed $LaPO_4$:Tb/$LaPO_4$:Eu (orange) NCs, (B) dry-mixed (green) NCs, together with pure $LaPO_4$:Tb (blue) and $LaPO_4$:Eu (red) NCs, and (C) wet-mixed (orange) NCs, together with pure $LaPO_4$:Tb (blue) and $LaPO_4$:Eu (red) NCs. The inset in panel A shows a close-up of the area between 450 and 500 nm. Clear differences are observed between the wet-mixed and dry-mixed NC excitation spectra. For the dry-mixed NCs, a typical $LaPO_4$:Eu excitation spectrum is observed, whereas both $LaPO_4$:Eu and $LaPO_4$:Tb excitation lines are observed in the case of wet-mixed NCs.

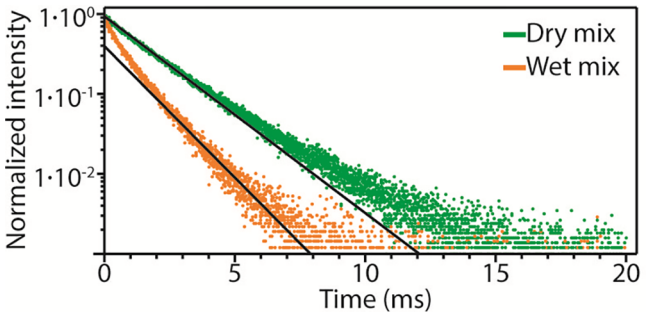

Figure 5. Photoluminescence decay curves of the Tb^{3+} $^5D_4$ state in dry-mixed and wet-mixed $LaPO_4$:Tb/$LaPO_4$:Eu NC composites. Black lines represent single-exponential fits, using decay times of 1.77 and 1.32 ms for the dry and wet mix, respectively. Excitation was at a λ of 355 nm, emission was monitored at a λ of 542 nm.

completeness, photoluminescence decay curves at elevated temperatures are shown in Figure S6. The temperature robustness of sensitization via IFRET of both emission

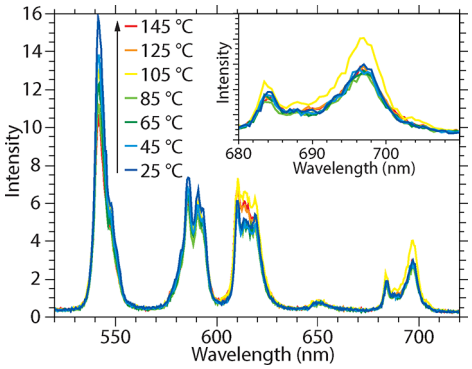

Figure 6. Temperature-dependent emission spectra on $LaPO_4$:Tb/$LaPO_4$:Eu wet-mixed NCs. The inset shows a close-up of the Eu^{3+} emission between 680 and 720 nm, which is almost constant over the measured temperature range. The sample was excited in the Tb^{3+} excitation line at a λ of 484.5 nm.

intensity and peak wavelength is a significant advantage of lanthanide-based multihost composites over, e.g., quantum dots or perovskite emitter materials for lighting applications.

To investigate IFRET between the sensitizer and emitter incorporated in different host lattices, we investigated the emission and excitation spectra of wet- and dry-mixed NC composites of $LaPO_4$:Tb and Y(V,P)O_4:Eu (Figure 7). Similar to what we observed for the $LaPO_4$:Tb/$LaPO_4$:Eu mixtures, only the wet-mixed sample shows Eu^{3+} emission at 698 nm upon Tb^{3+} excitation at 485 nm (Figure 7A,B). Many of the Tb^{3+} excitation lines are overlapping with the strong vanadate charge transfer band starting at 370 nm, but the Tb^{3+} excitation peak at 485 nm is clearly observed in the excitation spectrum of 698 nm Eu^{3+} emission for the wet-mixed sample but not for the dry-mixed sample (Figure 7D−F). Emission spectra for direct Eu^{3+} excitation at 395 nm are shown in Figure S7. Photoluminescence decay curves of the Tb^{3+} $^5D_4$ emission (Figure 7C) confirm nonradiative energy transfer in the wet-mixed sample. Taking the 1/e decay time leads to estimates of 9.2 ms^{-1} for the average IFRET rate and 78% for the IFRET efficiency. The oscillator strength of the acceptor and distance distribution affect the IFRET rate and are dependent on the host lattice of the Eu^{3+} ions. This could explain the difference between IFRET rates for $LaPO_4$:Tb/$LaPO_4$:Eu and $LaPO_4$:Tb/$YVPO_4$:Eu.

The observations depicted in Figure 7 provide evidence for efficient nonradiative energy transfer from Tb^{3+} in $LaPO_4$ to Eu^{3+} in $YVPO_4$, thereby demonstrating IFRET between dopants in different host materials for the first time. Even though IFRET efficiencies are generally lower than FRET efficiencies that can be observed for intraparticle energy transfer, near-unity efficiencies are not needed for many applications. To use Eu^{3+} as a red emitter in white LEDs, for example, IFRET efficiencies of only 20−30% are high enough to achieve high color rendering warm white light when a green emitter (such as $LaPO_4$:Tb or $Y_3Al_5O_{12}$:Ce) is used as the sensitizer (Figure S8). The reported efficiencies of 54% and 78% for LaPO4:Tb → LaPO4:Eu and LaPO4:Tb → YVPO4:Eu, respectively, are thus high enough to be interesting for these kinds of applications.

In conclusion, we have demonstrated IFRET between lanthanide-doped NCs. For $LaPO_4$:Tb/$LaPO_4$:Eu and $LaPO_4$:Tb/$YVPO_4$:Eu nanocrystals homogeneously intermixed at the nanoscale, we observed efficient sensitization of Eu^{3+}

https://dx.doi.org/10.1021/acs.jpclett.9b03764
J. Phys. Chem. Lett. 2020, 11, 689−695

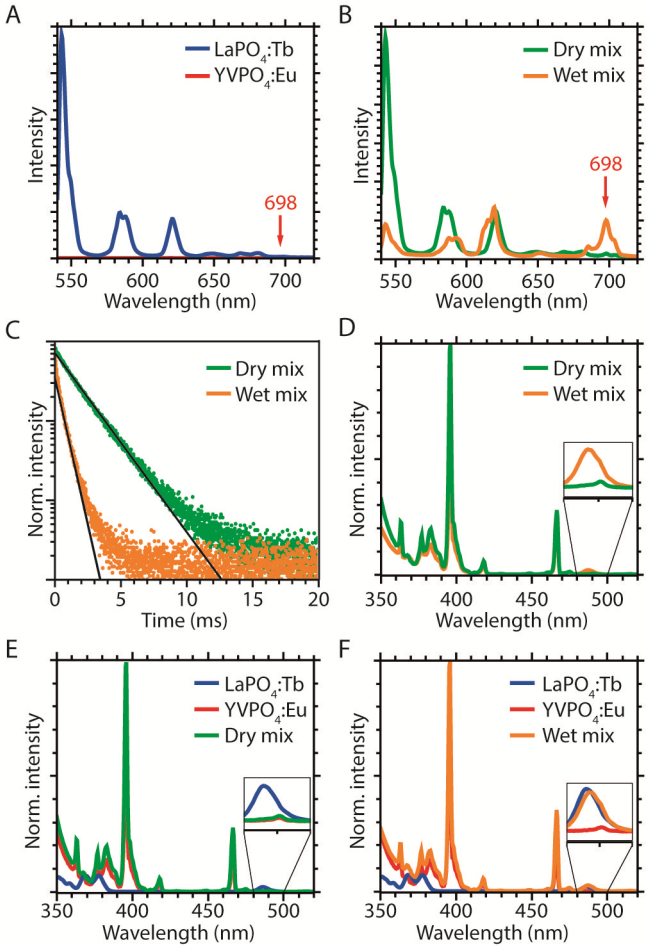

Figure 7. Photoluminescence measurements on $LaPO_4$:Tb/$YVPO_4$:Eu NCs. (A and B) Emission spectra upon Tb^{3+} excitation at a λ of 484.5 nm of (A) single-component $LaPO_4$:Tb (blue) and $YVPO_4$:Eu (red) NCs and (B) dry-mixed (green) and wet-mixed (orange) $LaPO_4$:Tb/$YVPO_4$:Eu NC composites. (C) Luminescence decay curves of the Tb^{3+} $^5D_4$ emission in dry-mixed (green) and wet-mixed (orange) $LaPO_4$:Tb/$YVPO_4$:Eu NC composites. Excitation at a λ of 355 nm, emission was monitored at a λ of 542 nm. Black lines represent single-exponential fits, using decay times of 1.95 and 0.61 ms for the dry and wet mix, respectively. (D–F) Excitation spectra of Eu^{3+} emission, monitored at a λ of 698 nm, of (D) dry-mixed (green) and wet-mixed (orange) $LaPO_4$:Tb/$YVPO_4$:Eu NC composites, (E) dry-mixed (green) NC composites, together with single-component $LaPO_4$:Tb (blue) and $YVPO_4$:Eu (red) NCs, and (F) wet-mixed (orange) NCs, together with single-component $LaPO_4$:Tb (blue) and $YVPO_4$:Eu (red) NCs. The insets show a close-up of the area between 480 and 500 nm.

emission upon Tb^{3+} excitation at 484.5 nm. Further support for IFRET is provided by excitation spectra of Eu^{3+} emission that clearly show the 485 nm Tb^{3+} excitation line and trace the full Tb^{3+} excitation spectrum in addition to the expected Eu^{3+} excitation lines. Furthermore, luminescence decay curves show acceleration of the Tb^{3+} $^5D_4$ emission in intermixed material, confirming nonradiative energy transfer from Tb^{3+} to Eu^{3+} acceptor ions in neighboring NCs. We envision that the concept of IFRET can be applied for a wide variety of sensitizer and emitter ions and in a wide variety of nanocrystal host materials. The flexibility in choice of host lattice for the sensitizer and emitter gives unprecedented freedom in independently tuning excitation and emission properties and opens up a whole new world of engineering of luminescent materials. For example, in new nanocomposites, efficient lanthanide emission can be generated upon visible light excitation, paving the way toward using lanthanides for a myriad of solid-state lighting applications.

EXPERIMENTAL METHODS

Materials. Lanthanum(III) chloride hexahydrate ($LaCl_3 \cdot 6H_2O$, 99.9% La, Brunschwig Chemie BV), europium(III) chloride hexahydrate ($EuCl_3 \cdot 6H_2O$, 99.9% trace metal basis, Sigma-Aldrich), terbium(III) chloride hexahydrate ($TbCl_3 \cdot 6H_2O$, 99.9% trace metal basis, Sigma-Aldrich), methyl alcohol (methanol, anhydrous, 99.8%, Sigma-Aldrich), tributyl phosphate (≥99.0%, Sigma-Aldrich), diphenyl ether (99%, Sigma-Aldrich), tributylamine (≥99.0%, Sigma-Aldrich), phosphoric acid (≥99.999%, Sigma-Aldrich), dihexyl ether (97%, Sigma-Aldrich), toluene (anhydrous, 99.8%, Sigma-Aldrich), an ammonium hydroxide solution (30%, Sigma-Aldrich), hydrogen peroxide (30 wt % in H_2O, Sigma-Aldrich), ethyl alcohol (ethanol, 30 ppm of H_2O, VWR international), hydrochloric acid (HCl, 37% in water, Sigma-Aldrich), and mixed phosphate/vanadate Y(V,P)O_4:Eu (YVPO4:Eu) nanoparticles (7% Eu, CAN GmbH, CANdot Series X) were used. HCl was diluted with water to 0.1 M, and all other chemicals were used as received.

Sample Preparation. $LaPO_4$:Eu^{3+} (10%) and $LaPO_4$:Tb^{3+} (40%) NPs with tributylamine ligands were synthesized using the procedure reported by the group of Haase.[36−39] In the case of LaPO4:Eu NPs, 9 mmol of $LaCl_3 \cdot 6H_2O$ and 1 mmol of $EuCl_3 \cdot 6H_2O$ were used, whereas for LaPO4:Tb, 6 mmol of $LaCl_3 \cdot 6H_2O$ and 4 mmol of $TbCl_3 \cdot 6H_2O$ were dissolved in approximately 10 mL of methanol until a clear solution was acquired. Then, 40 mmol of tributyl phosphate was added, and methanol was removed from the reaction mixture under vacuum using a Schlenk line. Thirty milliliters of diphenyl ether was added before the system was flushed with N_2. Next, water was released under vacuum at 105 °C before the reaction mixture was cooled to <50 °C and 40 mmol of tributylamine was added. Finally, 7.0 mL of a 2 M phosphoric acid solution in dihexyl ether was added. The reaction mixture was heated to 200 °C and left to react for 16 h before being cooled back to room temperature. The nanocrystals were collected by centrifuging and washed several times with toluene. The obtained nanoparticles were dried for further treatment and analysis. X-ray diffraction (XRD) patterns were measured for all nanocrystals to confirm the crystal structures before using them in the mixtures (Figure S9).

For the "wet-mixed" NC composites, 200 mg of dried $LaPO_4$:Eu or $YVPO_4$:Eu nanoparticles and 200 mg of dried $LaPO_4$:Tb nanoparticles were mixed in a vial and dispersed in 20 mL of water. The mixing was enhanced by sonication in an ultrasonic bath for 90 min. For the "dry-mixed" NC composites, 100 mg of dried $LaPO_4$:Eu nanoparticles and 100 mg of dried $LaPO_4$:Tb nanoparticles were separately dispersed in 20 mL of water or ethanol in different vials.

Ligands of the $LaPO_4$ nanoparticles were removed using a base-piranha treatment. The piranha solution was prepared by mixing an ∼3:1 weight ratio of a NH_4OH solution (30% in water, heated to 60 °C) and H_2O_2 (30% in water); 20−50 mL of this solution was added to the nanoparticle dispersions. The mixture was left to react at 70−80 °C for 90 min before the mixture was cooled to room temperature. The nanoparticles were re-collected by centrifugation and washed multiple times

https://dx.doi.org/10.1021/acs.jpclett.9b03764
J. Phys. Chem. Lett. 2020, 11, 689−695

with acidic ethanol (0.1 M HCl was added to ethanol to obtain a pH of 4).

The NC dispersions were dried at 120−150 °C in the oven. The mixed dispersion thus formed a wet-mixed NC composite. The dry NCs from the single-component dispersions were mixed with a mortar and pestle after drying to form dry-mixed NC composites, as reference samples.

Characterization. High-resolution transmission electron microscopy (HRTEM) images were taken using a JEOL ARM 200F instrument. The transmission electron microscope was probe corrected, equipped with a 100 mm^2 Centurio SDD EDX detector, and operated at 200 kV. Samples were prepared by dispersing the dry powder in ethanol, followed by sonication for 2 min. The samples were drop casted on a copper grid with holey carbon film.

Emission and excitation spectra were recorded using an Edinburgh Instruments FLS928 spectrofluorometer. A 450 W xenon lamp in combination with a monochromator was used for excitation, while the emitted light was collected using a R928 photomultiplier tube (λ = 400−850 nm). To record luminescence decay curves, the samples were excited using an optical parametric oscillator (OPO) system (Opotek Opolette HE 355 II), pumped by the third harmonic (355 nm) of a YAG:Nd laser, with a pulse width of 5 ns and a repetition rate of 20 Hz. For temperature-dependent measurements, a LINKAM cell was used, which has an optical window to monitor emission and excitation spectra during heating. All optical measurements were performed in reflection mode on optically thick powder samples.

■ ASSOCIATED CONTENT

Supporting Information

The Supporting Information is available free of charge at https://pubs.acs.org/doi/10.1021/acs.jpclett.9b03764.

Supporting simulations, XRD data, and additional (S)TEM, (S)TEM-EDX, and optical data (PDF)

■ AUTHOR INFORMATION

Corresponding Author

Marie Anne van de Haar − *Seaborough Research BV, Amsterdam, The Netherlands;* orcid.org/0000-0003-2581-6076; Email: m.vandehaar@seaborough.com

Other Authors

Anne C. Berends − *Seaborough Research BV, Amsterdam, The Netherlands*

Michael R. Krames − *Seaborough Research BV, Amsterdam, The Netherlands, and Arkesso LLC, Palo Alto, California*

Liudmyla Chepyga − *Utrecht University, Utrecht, The Netherlands*

Freddy T. Rabouw − *Utrecht University, Utrecht, The Netherlands;* orcid.org/0000-0002-4775-0859

Andries Meijerink − *Utrecht University, Utrecht, The Netherlands;* orcid.org/0000-0003-3573-9289

Complete contact information is available at: https://pubs.acs.org/10.1021/acs.jpclett.9b03764

Notes

The authors declare no competing financial interest.

■ ACKNOWLEDGMENTS

Marcel Verheijen from Eurofins Material Science Netherlands BV is gratefully acknowledged for technical support for HRTEM imaging and elemental mapping. Pradip Chakraborty and Jacobine van Hest are thanked for providing $LaPO_4$ nanoparticles, and Valerio Favale is thanked for photographs of the samples. This work is part of the research program Innovation Fund Chemistry (LIFT) with Project 731.017.401, which is (partly) financed by the Dutch Research Council (NWO). F.T.R. is supported by NWO Veni Grant 722.017.002 and by The Netherlands Center for Multiscale Catalytic Energy Conversion (MCEC), an NWO Gravitation program funded by the Ministry of Education, Culture and Science of the government of The Netherlands.

■ REFERENCES

(1) Feldmann, C.; Jüstel, T.; Ronda, C. R.; Schmidt, P. J. Inorganic Luminescent Materials: 100 Years of Research and Application. *Adv. Funct. Mater.* **2003**, *13*, 511−516.

(2) Bünzli, J. C. G.; Piguet, C. Taking Advantage of Luminescent Lanthanide Ions. *Chem. Soc. Rev.* **2005**, *34*, 1048−1077.

(3) Dwivedi, Y.; Zilio, S. C. Advances in Rare Earth Spectroscopy and Applications. *J. Nanosci. Nanotechnol.* **2014**, *14*, 1578−1596.

(4) Liu, G.; Chen, X. Chapter 233 Spectroscopic Properties of Lanthanides in Nanomaterials. *Handb. Phys. Chem. Rare Earths* **2007**, *37*, 99−169.

(5) Bünzli, J.-C. G.; Comby, S.; Chauvin, A.-S.; Vandevyver, C. D. B. New Opportunities for Lanthanide Luminescence. *J. Rare Earths* **2007**, *25*, 257−274.

(6) Van De Haar, M. A.; Werner, J.; Kratz, N.; Hilgerink, T.; Tachikirt, M.; Honold, J.; Krames, M. R. Increasing the Effective Absorption of Eu^{3++}-Doped Luminescent Materials towards Practical Light Emitting Diodes for Illumination Applications. *Appl. Phys. Lett.* **2018**, *112*, 132101.

(7) Krames, M. R. Rome Needs Red. *Arkesso* 2017.

(8) Setlur, A. A.; Comanzo, H. A.; Srivastava, A. M.; Beers, W. W. Spectroscopic Evaluation of a White Light Phosphor for UV-LEDs—$Ca_2NaMg_2V_3O_{12}$:Eu^{3++}. *J. Electrochem. Soc.* **2005**, *152*, H205−H208.

(9) Bandi, V. R.; Jayasimhadri, M.; Jeong, J.; Jang, K.; Lee, H. S.; Yi, S. S.; Jeong, J. H. Host Sensitized Novel Red Phosphor $CaZrSi_2O_7$:Eu^{3++} for near UV and Blue Led-Based White LEDs. *J. Phys. D: Appl. Phys.* **2010**, *43*, 395103.

(10) Xu, S.; Li, P.; Wang, Z.; Li, T.; Bai, Q.; Sun, J.; Yang, Z. Luminescence and Energy Transfer of Eu^{2++}/Tb^{3++}/Eu^{3++} in $LiBaBO_3$ Phosphors with Tunable-Color Emission. *J. Mater. Chem. C* **2015**, *3*, 9112−9121.

(11) Setlur, A. A. Sensitizing Eu^{3++} with Ce^{3++} and Tb^{3++} to Make Narrow-Line Red Phosphors for Light Emitting Diodes. *Electrochem. Solid-State Lett.* **2012**, *15*, J25.

(12) Ogiegło, J. M.; Zych, A.; Ivanovskikh, K. V.; Jüstel, T.; Ronda, C. R.; Meijerink, A. Luminescence and Energy Transfer in $Lu_3Al_5O_{12}$ Scintillators Co-Doped with Ce^{3++} and Tb^{3++}. *J. Phys. Chem. A* **2012**, *116*, 8464−8474.

(13) Babin, V.; D. Oskam, K.; Vergeer, P.; Meijerink, A. The Role of Pb^{2++} as a Sensitizer for Gd^{3++}−Eu^{3++} Downconversion Couple in Fluorides. *Radiat. Meas.* **2004**, *38*, 767−770.

(14) Krishna Reddy, D. V.; Taherunnisa, S.; Lakshmi Prasanna, A.; Sambasiva Rao, T.; Veeraiah, N.; Rami Reddy, M. Enhancement of the Red Emission of Eu^{3++} by Bi^{3++} Sensitizers in Yttrium Alumino Bismuth Borosilicate Glasses. *J. Mol. Struct.* **2019**, *1176*, 133−148.

(15) De Vries, A. J.; Hazenkamp, M. F.; Blasse, G. On the Gd^{3++} Luminescence and Energy Migration in Li(Y, Gd)F_4-Tb^{3++}. *J. Lumin.* **1988**, *42*, 275−282.

(16) Ogiegło, J. M.; Zych, A.; Jüstel, T.; Meijerink, A.; Ronda, C. R. Luminescence and Energy Transfer in $Lu_3Al_5O_{12}$ Scintillators Co-Doped with Ce^{3++} and Pr^{3++}. *Opt. Mater. (Amsterdam, Neth.)* **2013**, *35*, 322−331.

(17) Ding, M.; Chen, D.; Wan, Z.; Zhou, Y.; Zhong, J.; Xi, J.; Ji, Z. Achieving Efficient Tb^{3++} Dual-Mode Luminescence via Gd-Sublattice-Mediated Energy Migration in a $NaGdF_4$Core-Shell Nanoarchitecture. *J. Mater. Chem. C* **2015**, *3*, 5372−5376.
(18) Liu, L.; Zhang, N.; Leng, Z.; Liang, Y.; Li, R.; Zou, L.; Gan, S. Highly Bright Multicolour Emission through Energy Migration in Core/Shell Nanotubes. *Dalt. Trans.* **2015**, *44*, 6645−6654.
(19) Tao, L.; Zhao, Y.; Li, J. Photon Upconversion in Yb/Tb Co-Sensitized Core-Shell Nanocrystals by Interfacial Energy Transfer. *Opt. Mater. Express* **2017**, *7*, 1022.
(20) Zhou, B.; Tao, L.; Chai, Y.; Lau, S. P.; Zhang, Q.; Tsang, Y. H. Constructing Interfacial Energy Transfer for Photon Up- and Down-Conversion from Lanthanides in a Core−Shell Nanostructure. *Angew. Chem., Int. Ed.* **2016**, *55*, 12356−12360.
(21) Zhou, B.; Yang, W.; Han, S.; Sun, Q.; Liu, X. Photon Upconversion Through Tb^{3++}-Mediated Interfacial Energy Transfer. *Adv. Mater.* **2015**, *27*, 6208−6212.
(22) Wang, F.; Deng, R.; Wang, J.; Wang, Q.; Han, Y.; Zhu, H.; Chen, X.; Liu, X. Tuning Upconversion through Energy Migration in Core-Shell Nanoparticles. *Nat. Mater.* **2011**, *10*, 968−973.
(23) Zuo, J.; Sun, D.; Tu, L.; Wu, Y.; Cao, Y.; Xue, B.; Zhang, Y.; Chang, Y.; Liu, X.; Kong, X.; et al. Precisely Tailoring Upconversion Dynamics via Energy Migration in Core−Shell Nanostructures. *Angew. Chem., Int. Ed.* **2018**, *57*, 3054−3058.
(24) Ding, L.; Karasz, F. E. Color Tuning and Efficiency Enhancement through Interfacial Energy Transfer and Thickness Control in Light-Emitting Diodes. *J. Appl. Phys.* **2004**, *96*, 2272−2277.
(25) Pokhrel, M.; Valdes, C.; Mao, Y. Ultraviolet Upconversion Enhancement in Triply Doped $NaYF_4$:Tm^{3++}, Yb^{3++} particles: The Role of Nd^{3++} or Gd^{3++}Co-Doping. *Opt. Mater. (Amsterdam, Neth.)* **2016**, *58*, 67−75.
(26) Huang, X. Realizing Efficient Upconversion and Down-Shifting Dual-Mode Luminescence in Lanthanide-Doped $NaGdF_4$ Core-Shell-Shell Nanoparticles through Gadolinium Sublattice-Mediated Energy Migration. *Dyes Pigm.* **2016**, *130*, 99−105.
(27) Fischer, S.; Baur, F.; Jüstel, T. Suppression of Metal-to-Metal Charge Transfer Quenching in Ce^{3++} and Eu^{3++} comprising Garnets by Core-Shell Structure. *J. Lumin.* **2018**, *203*, 467−472.
(28) Zeng, P.; Wei, X.; Zhou, S.; Yin, M.; Chen, Y. Evaluation of Critical Distances for Energy Transfer between Pr^{3++} and Ce^{3++} in Yttrium Aluminium Garnet. *J. Appl. Phys.* **2016**, *120*, 093104.
(29) Rodrigues, M. O.; Dutra, J. D. L.; Nunes, L. A. O.; De Sá, G. F.; De Azevedo, W. M.; Silva, P.; Paz, F. A. A.; Freire, R. O.; A. Júnior, S. Tb^{3++}-Eu^{3++} Energy Transfer in Mixed-Lanthanide-Organic Frameworks. *J. Phys. Chem. C* **2012**, *116*, 19951−19957.
(30) Blasse, G. Optical Electron Transfer between Metal Ions and Its Consequences. In *Complex Chemistry*; Springer: Berlin, 1991; pp 153−187.
(31) Setlur, A. A.; Shiang, J. J. Quantitative Analysis of Electron Transfer between $Ce^{3++}(^5d_1)$ and Yb^{3++}/Eu^{3++} Ions in $Y_3Al_5O_{12}$ and $Lu_2Si_2O_7$. *J. Phys. Chem. C* **2010**, *114*, 2792−2798.
(32) Wang, F.; Deng, R.; Wang, J.; Wang, Q.; Han, Y.; Zhu, H.; Chen, X.; Liu, X. Tuning Upconversion through Energy Migration in Core-Shell Nanoparticles. *Nat. Mater.* **2011**, *10*, 968−973.
(33) Sarkar, S.; Meesaragandla, B.; Hazra, C.; Mahalingam, V. Sub-5 Nm Ln^{3++}-Doped $BaLuF_5$ Nanocrystals: A Platform to Realize Upconversion via Interparticle Energy Transfer (IPET). *Adv. Mater.* **2013**, *25*, 856−860.
(34) Rabouw, F. T.; Den Hartog, S. A.; Senden, T.; Meijerink, A. Photonic Effects on the Förster Resonance Energy Transfer Efficiency. *Nat. Commun.* **2014**, *5*, 1−6.
(35) Vergeer, P.; Vlugt, T. J. H.; Kox, M. H. F.; den Hertog, M. I.; Van Der Eerden, J. P. J. M.; Meijerink, A. Quantum Cutting by Cooperative Energy Transfer in $Yb_xY_{1-x}PO_4$:Tb^{3++}. *Phys. Rev. B: Condens. Matter Mater. Phys.* **2005**, *71*, 014119.
(36) Riwotzki, K.; Meyssamy, H.; Schnablegger, H.; Kornowski, A.; Haase, M. Liquid-Phase Synthesis of Colloids and Redispersible Powders of Strongly Luminescing LaPO4:Ce, Tb Nanocrystals. *Angew. Chem., Int. Ed.* **2001**, *40*, 573−576.
(37) Lehmann, O.; Kömpe, K.; Haase, M. Synthesis of Eu3+-Doped Core and Core/Shell Nanoparticles and Direct Spectroscopic Identification of Dopant Sites at the Surface and in the Interior of the Particles. *J. Am. Chem. Soc.* **2004**, *126*, 14935−14942.
(38) Riwotzki, K.; Meyssamy, H.; Kornowski, A.; Haase, M. Liquid-Phase Synthesis of Doped Nanoparticles: Colloidal of Luminescing $LaPO_4$:Tb Particles with a Narrow Particle Size Distribution. *J. Phys. Chem. B* **2000**, *104*, 2824−2828.
(39) Lehmann, O.; Meyssamy, H.; Kompe, K.; Schnablegger, H.; Haase, M. Synthesis, Growth, and Er^{3++} Luminescence of Lanthanide Phosphate Nanoparticles. *J. Phys. Chem. B* **2003**, *107*, 7449−7453.

https://dx.doi.org/10.1021/acs.jpclett.9b03764
J. Phys. Chem. Lett. 2020, 11, 689−695